Optical properties of ZnSe and its modeling

Charles C. Kim and S. Sivananthan
University of Illinois at Chicago, Microphysics Laboratory, Physics Department, 845 West Taylor Street, Chicago, Illinois 60607-7059
(Received 22 June 1995; revised manuscript received 18 September 1995)

Spectral data for a ZnSe film grown on GaAs(100) are obtained at room temperature by spectroscopic ellipsometry (SE) in the photon energy range between 1.5 eV and 6 eV in steps of 5 meV. The optical dielectric function for bulk ZnSe is successfully extracted from the spectral data utilizing a multilayer analysis. The resultant data are better than previous data in that (1) the real part of the dielectric function below the band gap decreases smoothly following closely Marple's data obtained by the beam deviation method, which is more reliable than SE in this energy range, (2) the data reveal four distinctive critical point structures at E_0, $E_0+\Delta_0$, E_1, and $E_1+\Delta_1$, as is expected from the band structure, and (3) the maximum value of the imaginary part of the dielectric function in the E_1 region is highest among the reported data. The resultant data are expressed as a function of critical-point parameters and photon energies using our model, which is more generally valid than other models. This enables us to calculate the optical dielectric function not only over the entire photon energy range of the given spectral data, but also below and somewhat above the given spectral range. The excitonic effects apparently present in the spectral data are incorporated in our model. This enables us to determine excitonic parameters. The excitonic binding energy at E_0 is found to be 13 meV at room temperature.

I. INTRODUCTION

ZnSe has been an attractive material for various optoelectronic devices,[1] especially for laser diodes,[2,3] in which it is used as the binary end compound of alloy systems, such as $Zn_{1-x}Cd_xSe$ and $Zn_{1-x}Mg_xS_ySe_{1-y}$. Recently, it has been reported that laser diodes based on these materials operate in a continuous-wave mode for an hour at room temperature.[4] A knowledge of refractive indices and absorption coefficients of these materials is important in the design and analysis of heterostructure lasers and other waveguiding semiconductor devices.[5] A knowledge of dielectric functions is also valuable in controlling the thickness and alloy composition in real time.[6] In such an application, it is essential to calculate those values as a function of wavelength and alloy composition. Spectroscopic ellipsometry (SE) is an excellent technique, which determines the spectral dependence of the dielectric function, $\epsilon(\omega)=\epsilon_1(\omega)+i\epsilon_2(\omega)$. However, values for $\epsilon(\omega)$ obtained from the experimental data have a serious deficiency: they are not expressed as a function of critical-point energies E_j, or even of photon energy $\hbar\omega$. The SE data in conjunction with modeling, however, allows one to calculate the dielectric function as a function of photon energy, temperature, and alloy composition.

The optical properties of ZnSe have been extensively tabulated by Ward.[7] None of them, however, was determined by SE, which does not require the use of the Kramers-Kronig relationship to determine the optical dielectric function. Adachi and Taguchi measured the optical properties of bulk ZnSe in the photon energy range between 1.5 and 5.3 eV, using a commercially available spectroscopic ellipsometer.[8] The overlayer effect, however, was not removed in their data. They modeled their spectral data using a model dielectric function, in which the contribution of excitons is very large—for example, the entire contribution to $\epsilon_2(\omega)$ between E_1 and $E_1+\Delta_1$. Recently, Kim *et al.*[9] reported SE data between 1.5 eV and 6 eV for ZnSe films grown on GaAs. Due to successful etching, the optical dielectric function that they obtained in the E_1 region is the highest among all previous data, suggesting that it may be the best representation for bulk ZnSe. However, the real part of the optical dielectric function that they reported is not well defined near the band gap and does not show a smooth decrease below the band gap as it should.

ZnSe films were grown on GaAs (100) by the use of molecular beam epitaxy. Their spectral data were measured in steps of 5 meV from 1.5 eV to 6 eV by spectroscopic ellipsometry.[10] The data of some samples revealed a distinctive critical-point structure at E_0, $E_0+\Delta_0$, E_1 and $E_1+\Delta_1$, whereas those of others did not. The best set of data, which revealed four distinctive critical-point structures, was chosen for this work. The effect of the overlayer and substrate was obvious in the spectral data, and the optical properties of bulk ZnSe were extracted from the spectral data, using a multilayer structure analysis.[11,12] The detailed procedures are the subject of another paper, which will be reported elsewhere. The resultant modified data are better than any previous data in that (1) the real part of the dielectric function below the band gap decreases smoothly following closely Marple's data obtained by the beam deviation method, which is more reliable than SE in this energy range, (2) the data reveal four distinctive critical-point structures at E_0, $E_0+\Delta_0$, E_1, and $E_1+\Delta_1$, as is expected from the band structure, and (3) the maximum value of the imaginary part of the dielectric function in the E_1 region is highest among the reported values. This point is discussed more fully at the end of Sec. II.

The resultant modified data were adopted for modeling. Our model for the optical dielectric function has proven to be more generally valid than any other model[13] and has been successfully applied to fit the spectral data of the alloy system $Ga_{1-x}Al_xAs$.[14] Recently, we have improved our ap-

proach in using this model, so that the resultant calculation for $\epsilon(\omega)$ exactly satisfies the Kramers-Kronig relationship.[15] The optical properties of bulk ZnSe at room temperature revealed a sharp structure at E_0 and at $E_0+\Delta_0$, due to excitons. The optical line shape due to excitons, however, was not incorporated in the original model. Thus, we developed an exciton line shape and properly incorporated it in our model. This enabled us to determine the excitonic parameters accurately, leading to 13 meV for the room-temperature exciton binding energy at E_0. The modeling also led us to calculate $\epsilon(\omega)$ not only over the given range of the spectral data used for the fit, but also beyond that range. The values for $\epsilon(\omega)$ below the lower limit of the spectral data are very close to those obtained by Marple.[16] The values for $\epsilon(\omega)$ above the upper limit appear reasonable in that the maximum value of $\epsilon_2(\omega)$ in the E_2 region is on the order of 15, which is close to the theoretically calculated value.[17]

In Sec. II, we explain the experimental details and the data preparation for bulk ZnSe. The data are compared with previous data. In Sec. III, we develop the exciton line shape and incorporate it into our model. In Sec. IV, we use the model to determine the critical-point parameters, the excitonic parameters, and other constant parameters by fitting the data from 1.5 eV to 6 eV. Then, we calculate $\epsilon(\omega)$ between 0.2 eV and 8 eV. In Sec. V, we present our conclusions.

II. EXPERIMENT

ZnSe layers of high quality have been grown on GaAs (100) substrates by molecular beam epitaxy (MBE) in a RIBER 2300 system. The details of growth were reported previously.[18] Briefly, the substrates were chemically etched in a 4:1:1 solution of H_2SO_4:H_2O_2:H_2O, rinsed in HCl and H_2O and then loaded into the UHV system. The native oxide was desorbed *in situ* by heating the substrate to about 600 °C. Once the desorption was complete the substrate was cooled down with Zn or Se flux and ZnSe growth was initiated at 350 °C, using elemental Zn and Se. The growth rate is on the order of 1 Å/s. The quality of grown layers was routinely checked by x-ray rocking-curve and photoluminescence measurements. The full width at half maximum of the double-crystal x-ray rocking curve for ZnSe/GaAs was as narrow as 27 arcsec. Low-temperature photoluminescence measurement showed free exciton linewidths as low as 0.93 meV.

Our spectroscopic ellipsometer uses a photoelastic modulator. It has been improved to measure the dielectric function, especially in the photon energy range up to 6 eV, so that the E_1 structure of wide-band-gap materials, which occurs around 5 eV, may be obtained. The experimental setup, procedure, and method of data reduction were reported previously.[13] The measurement was done in steps of 5 meV from 1.5 eV to 6 eV, using configuration II, as defined by Bermudez and Ritz,[19] and zone averaging, which is made easier with our system and improves the accuracy. The sample surface was gently rinsed with methanol before the measurement. The dotted lines in Fig. 1 show the spectral data for the ZnSe film grown on a GaAs substrate. Four critical-point (CP) structures at E_0, $E_0+\Delta_0$, E_1, and $E_1+\Delta_1$ are apparent in the spectral data. The CP structures at $E_0+\Delta_0$ and $E_1+\Delta_1$ are weaker than those at E_0 and E_1

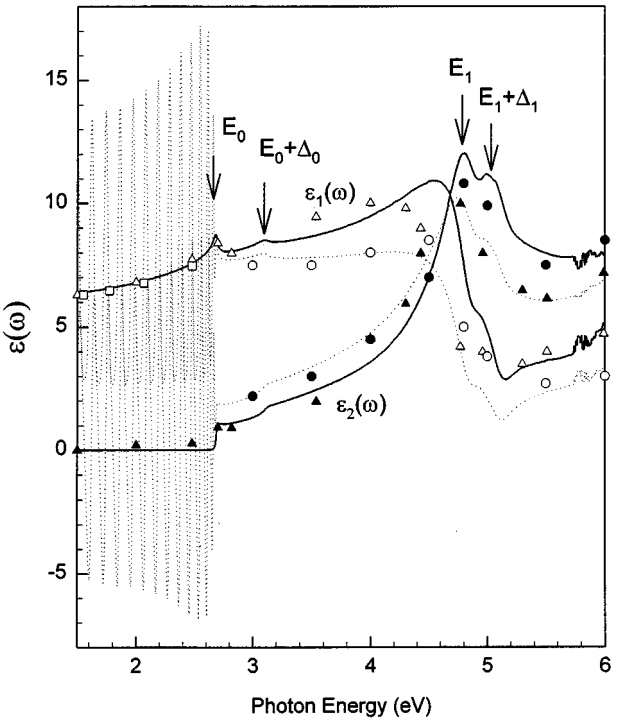

FIG. 1. Spectral data of ZnSe. The dotted lines show the spectral data for the system overlayer/ZnSe/GaAs. The solid lines show $L(\omega_j)=L_1(\omega_j)+L_2(\omega_j)$, which are extracted to represent the dielectric function of bulk ZnSe. The open and closed triangles show the real and imaginary parts of the dielectric function for bulk ZnSe obtained by Cardona (Ref. 26). The open squares show the real part of the dielectric function for bulk ZnSe obtained by Marple (Ref. 16). The open and solid circles show the real and imaginary parts of the dielectric function for bulk ZnSe obtained by Kim *et al.* (Ref. 9).

and are not observed for samples with poor quality. The data show a clear E_1 and $E_1+\Delta_1$ structure around 5 eV, revealing that the sample has a high degree of crystalline quality. The optical dielectric function for bulk ZnSe,[8] grown by a recrystallization traveling-heater method,[20] did not show a clear CP structure at $E_1+\Delta_1$, indicating that the crystalline quality of ZnSe is better for a thin film grown on GaAs by molecular beam epitaxy than for a bulk crystal. The interference pattern seen below the band gap of ZnSe is expected for a film/substrate system and carries information on the film thickness. Above the band gap no interference occurs, due to the high absorption coefficient of ZnSe, but the values around the E_1 region are generally reduced, due to a thin overlayer.

To obtain the optical properties for bulk ZnSe, the effect of the overlayer and substrate was removed numerically from the spectral data for the overlayer/ZnSe/GaAs system. The details will be reported elsewhere. The procedures for removing the effect of one layer from the spectral data for a multilayered structure have been described previously.[11,12] In this approach, the resultant dielectric function is extracted point by point, given the information on the thickness and the dielectric function of the layer to be removed. First, the overlayer effect is removed. The overlayer effect consists of the effect of the oxide layer and of surface roughness. Their natures are different, but their effect on the dielectric func-

tion is similar, except for a slight change in the thickness.[21] To simplify the calculation, we ascribed the overlayer effect entirely to the effect of an oxide layer. The optical dielectric function for the oxide layer on ZnSe, supposedly $ZnSeO_2$, is not known. As a trial, both the optical dielectric function of SiO_2 (Ref. 22) and that of $GaAsO_2$ (Ref. 23) were tried, with no significant difference observed below 4 eV. Thus, our lack of knowledge of the dielectric function of $ZnSeO_2$ did not pose a serious hindrance in determining the optical dielectric function of bulk ZnSe below 4 eV. However, a significant difference on the order of 1 was observed above 4 eV. Assuming that the II-VI compound has optical properties closer to those of the III-V compound than to those of the elemental semiconductor, the dielectric function of $GaAsO_2$ was adopted to represent that of $ZnSeO_2$, as well as the surface roughness of ZnSe. The overlayer thickness was determined from evaluating the average values, $\langle \epsilon_2(\omega) \rangle$, obtained for $\epsilon_2(\omega)$ between the interference peaks below the band gap of ZnSe, since $\langle \epsilon_2(\omega) \rangle$ becomes zero in the absence of an overlayer.[24] Assuming a 30 Å $GaAsO_2$ for the overlayer produced $\langle \epsilon_2(\omega) \rangle$ values close to zero. Coincidentally 30 Å is a typical thickness for the native oxide layer of GaAs.[25]

After removing the overlayer effect, the effect of the GaAs substrate was removed. The optical dielectric function for GaAs is well known and was adopted from previous work.[13] Knowing the film thickness accurately and choosing proper initial values for the dielectric function of the film are the keys to obtain the right solution. They were determined as follows. We have developed a simple model, which describes the dielectric function of bulk semiconductors around the band gap. Then the total dielectric function for the film/substrate system was constructed, using this model for the film and the known values for GaAs. In this approach, the thickness was treated as a parameter. A film thickness of about 2 μm was deduced from the first peak position at 1.64 eV, the next-nearest peak position at 1.76 eV, and the average value of the refractive index, as determined by Marple[16] in this spectral region, and was initially used in the fitting. The best fit led to a film thickness of 1.937 μm. This result was used in the point by point solution. For other assumed thicknesses, $\epsilon_1(\omega)$ became further away from the data of Marple, or even unphysical.

The solid lines in Fig. 1 show the real and imaginary parts of the extracted optical dielectric function, $L(\omega_j)=L_1(\omega_j)+iL_2(\omega_j)$, obtained for bulk ZnSe. The open and solid triangles show the results of Cardona,[26] which were tabulated by Ward.[7] The open squares show the results of Marple,[16] also tabulated by Ward. The numerical data of Kim *et al.*[9] were not available to us. Several points are obtained from their graphical data and are presented by the open and solid circles. In general, $L(\omega_j)$ is similar to the data of Adachi *et al.* and Kim *et al.*, except for several points discussed below. $L_1(\omega_j)$ below the band gap is slightly higher than the values found by Marple and very close to the values found by Cardona. On the other hand, the values determined for $\epsilon_1(\omega)$ by Kim *et al.* are even higher than ours. Our experience suggests that their results could arise from the wrong value for the film thickness and/or ill-conditioned initial values for $\epsilon_1(\omega)$. We wonder why our values for $\epsilon_1(\omega)$ are slightly higher than those of Marple. For example, ours and his at 2.5 eV are 7.635 and 7.515, respectively. (See also Table I.) We conjecture two reasons for such discrepancies. SE is a reflection technique; thus, the higher values might have been caused by the effect of surface termination on the reflection coefficients.[13,27] Otherwise, they may reflect the quality difference between two materials. Around 3 eV, $L_2(\omega_j)$ is on the order of 1.2, close to the values found by Cardona, but lower than those found by Adachi *et al.* and by Kim *et al.*, which are on the order of 2. Notice that the values found by Adachi *et al.* and by Kim *et al.* are close to ours before the effect of the oxide layer is removed. The difference between our values and the values found by Adachi *et al.* may be due to the effect of the surface overlayer. The difference between our values and the values found by Kim *et al.* may be due to surface roughening during chemical etching, or due to the surface roughness inherent in the sample. Above the band gap, $L(\omega_j)$ is closer to the values found by Cardona up to 4 eV, and begins to show a difference from his values from 4 eV to 6 eV. It is known that the optical dielectric function for bulk semiconductors is better represented by higher experimental values of $\epsilon_2(\omega)$ in the E_2 region,[28] or in the E_1 region for wide-band-gap materials.[9] The maximum value of $\epsilon_2(\omega)$ in the E_1 region found by Adachi *et al.*, Kim *et al.*, and ourselves are on the order of 11.3, 11, and 12, respectively.

TABLE I. Values for $\epsilon_1(\omega)$ at 1.5 eV, 2.5 eV, and 2.6 eV, obtained from $L_1(\omega_j)$ and its fit. They are also compared with the data by Marple (Ref. 16).

	This work		
Photon energy (eV)	Data	Fit	Ref. 16
1.5	6.379	6.183	6.277
2.5	7.635	7.532	7.515
2.6	8.003	7.936	7.777

III. THEORY

The optical dielectric function[13,14] of solid state materials with Lorentzian line broadening is given by the equation

$$\epsilon(\omega)=1-\frac{8\pi\hbar^2e^2}{m^2}\int\frac{W(E)dE}{E^2}\left[\frac{1}{\hbar\omega-E+i\Gamma}-\frac{1}{\hbar\omega+E+i\Gamma}\right], \tag{1}$$

where

$$W(E)=\sum_{c,v}W_{cv}(E)=\sum_{c,v}P_{cv}(E)^2J_{cv}(E),$$

c and v stand for conduction and valence bands, respectively, $E\equiv E_{cv}(\mathbf{k})$ is the energy difference between a pair of bands at the point $\mathbf{k}$ in the Brillouin zone, $J_{cv}(E)$ is the joint density of states between the pair of bands, and $P_{cv}(E)$ is the weighted-average matrix element of the momentum operator between states differing in energy by E. Similarly, the optical dielectric function of solid state materials with Gaussian broadening is given by the equation

$$\epsilon(\omega)=1+i\frac{8\pi\hbar^2e^2}{m^2}\int\frac{W(E)dE}{E^2}\left[\int_0^\infty ds e^{i(\hbar\omega-E+2i\tau^2s)s}-\int_0^\infty ds e^{i(\hbar\omega+E+2i\tau^2s)s}\right], \quad (2)$$

where τ is the root-mean-square scattering t matrix. Our model is based on these two equations: Eq. (1) and Eq. (2). The model is obtained first by constructing $W(E)$ and then by integrating it over E analytically. Last, the excitonic line shape is added to produce the final model.

A. Optical line shape for excitons

Excitonic effects are usually stronger in II-VI compounds than in III-V compounds, because of the larger binding energies due to the smaller values of the static dielectric constant. The excitons in the neighborhood of the lowest direct band edge significantly change the optical response.[29,30] These effects are also obvious in $L_2(w_j)$ near E_0 and $E_0+\Delta_0$ and require the incorporation of excitonic effects in our existing model. For illustration, the resultant fit to $L_2(w_j)$ near E_0 without including the excitonic effect will be shown first. The fit is performed by minimizing the root-mean-square (rms) fractional error,

$$\sigma=\frac{1}{4}\sum_{n=0}^{n=3}\sigma_n, \quad (3)$$

where

$$\sigma_n^2=\frac{\Sigma_j|[f_j]^{(n)}_{\rm num}-[s_j]^{(n)}_{\rm num}|^2}{\Sigma_j|[s_j]^{(n)}_{\rm num}|^2} \quad (4)$$

f_j denotes a theoretical model, s_j denotes the data, the superscript n denotes an nth order derivative, and the subscript num denotes numerical differentiation. The numerical differentiation is performed using a formula suggested by Savitz and Golay.[31] Notice that the numerical differentiation is applied both to the model and to the data, so as to compensate for numerical distortion.[32,33]

The spectral data near the band gap are usually modeled by a 3D M_0 type CP at E_0. This has the form

$$W(E)=p_0\sqrt{E-E_0}, \quad (5)$$

where p_0 is a constant. Substituting Eq. (5) into Eq. (1) leads to

$$\epsilon(\omega)=1-\frac{8\pi\hbar^2e^2}{m^2}p_0H_0(\omega), \quad (6)$$

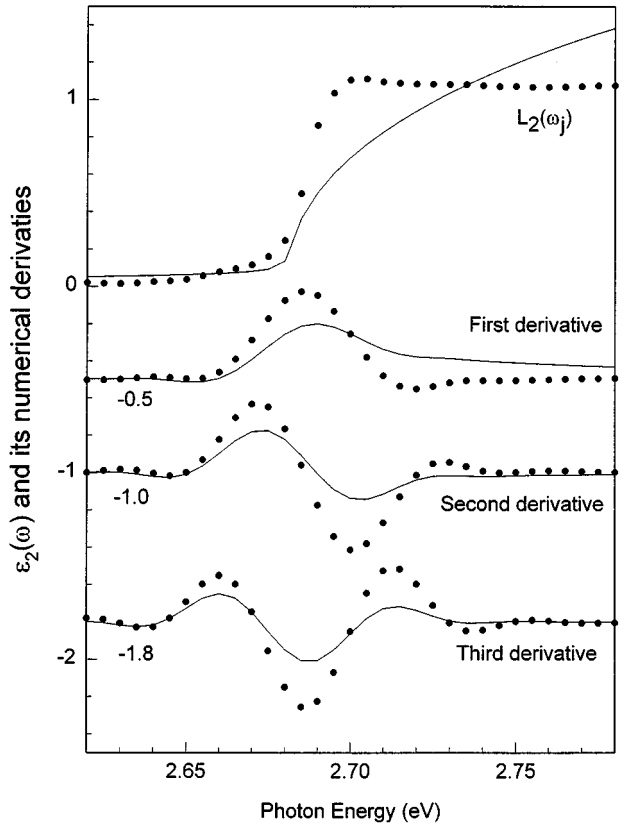

FIG. 2. Fit to $L_2(\omega_j)$ and its derivatives by the use of Eq. (6). The solid lines are the fits. The closed circles (●) are $L_2(\omega_j)$ and its numerical derivatives. The first three derivatives shown are normalized and shifted for comparison. σ is 54%.

where $H_0(\omega)$ has been defined previously.[13] Figure 2 shows the best fit of Eq. (6) to $L_2(w_j)$ and its derivatives, where p_0, E_0, and Γ_0 are free parameters. Here, $L_2(w_j)$ and its derivatives, not $L(w_j)$ and its derivatives, are chosen, since $L_1(w_j)$ has a contribution far above the band gap and Eq. (6) alone is not suitable to describe $L_1(w_j)$. The solid lines and closed circles in Fig. 2 show the best fit and the spectral data, respectively. σ is 55%. The model has a square root singularity as intended, but $L_2(w_j)$ shows a sharper structure, due to the excitonic effects, indicating that a 3D M_0 type CP alone is not sufficient for describing $L_2(w_j)$ near the band gap.

The formalism for the excitonic contribution to the imaginary part of the optical dielectric function is given by Elliott.[34] For Lorentzian line broadening, the discrete series of exciton lines below a given critical-point energy E_i gives a contribution

$$\epsilon_{\rm ex}(\omega)[E_i]=-C_{\rm ex}\sum_{n=1}^{\infty}\frac{1}{n^3}\left[\frac{1}{\hbar\omega-(E_i-E_{\rm ex}/n^2)+i(\Gamma^{(0)}_{\rm ex}-\Gamma^{(1)}_{\rm ex}/n^2)}-\frac{1}{\hbar\omega+(E_i-E_{\rm ex}/n^2)+i(\Gamma^{(0)}_{\rm ex}-\Gamma^{(1)}_{\rm ex}/n^2)}\right]$$
$$=-\frac{C_{\rm ex}}{2}\left[\frac{1}{E_{\rm ex}-i\Gamma^{(1)}_{\rm ex}}\ln\frac{\hbar\omega-E_i+i\Gamma^{(0)}_{\rm ex}}{\hbar\omega-(E_i-E_{\rm ex})+i(\Gamma^{(0)}_{\rm ex}-\Gamma^{(1)}_{\rm ex})}+\frac{1}{E_{\rm ex}+i\Gamma^{(1)}_{\rm ex}}\ln\frac{\hbar\omega+E_i+i\Gamma^{(0)}_{\rm ex}}{\hbar\omega+(E_i-E_{\rm ex})+i(\Gamma^{(0)}_{\rm ex}-\Gamma^{(1)}_{\rm ex})}\right], \quad (7)$$

TABLE II. Values of the critical point and excitonic parameters at E_0 and $E_0+\Delta_0$. They are determined through the fitting as described in the text.

	$H_0(\omega)$			$\epsilon_{ex}(\omega)$			
CP	$8\pi\hbar^2e^2p_0/m^2$	E_i (eV)	Γ_i (meV)	$C_{ex}/2$	E_{ex} (meV)	$\Gamma_{ex}^{(0)}$ (meV)	$\Gamma_{ex}^{(1)}$(meV)
E_0	8.71	2.711	5	0.020	13	40	35
$E_0+\Delta_0$	7.10	3.139	37	0.023	13	120	83

where $\Gamma_{ex}^{(0)}$ and $\Gamma_{ex}^{(1)}$ are exciton linewidths, C_{ex} is the exciton strength parameter, E_{ex} is the exciton binding energy. Notice that $\Gamma_{ex}^{(1)}$ takes into account the variation of exciton linewidth as n varies. It has been known that the exciton linewidth increases as n increases. We conjecture that $\Gamma_{ex}^{(1)}$ is inversely proportional to n^2. In this scheme, $\Gamma_{ex}^{(0)}-\Gamma_{ex}^{(1)}$ is the line width of the fundamental exciton. This quantity $\Gamma_{ex}^{(1)}$ was not introduced, or equivalently was set to zero, in the model for the exciton line shape proposed by Adachi and Taguchi.[8] Besides, their exciton line shape considered only the first order term instead of summing over n. The excitonic line shape of Eq. (7) is asymmetrical if $\Gamma_{ex}^{(1)}\neq 0$, but becomes symmetrical as $\Gamma_{ex}^{(1)}$ approaches zero. The peak position shifts down from E_i by an amount E_{ex}. Equation (1) is unique in that it not only describes the spectral data, but also its derivatives simultaneously. So is Eq. (7), because it preserves the correct analytical properties of the excitonic effect.

Since the effect of excitons is additional, not substitutional, to the optical dielectric function arising from electronic transitions between the bands, $H_0(\omega)$ and $\epsilon_{ex}(\omega)$ are combined to describe the spectral data near E_0. The combination leads to the model

$$\epsilon(\omega)=1-\frac{8\pi\hbar^2e^2}{m^2}p_0H_0(\omega)+\epsilon_{ex}(\omega)[E_0]. \tag{8}$$

This equation contains four more parameters than Eq. (6). The fit to $L_2(\omega_j)$ was performed by minimizing σ. During the fitting, E_{ex} was initially fixed at 17 meV (Ref. 35) and was gradually released. If the initial value for E_{ex} were ill-conditioned, E_{ex} increased indefinitely for a better fit, leading to unphysical values. The best fit led to 13 meV for E_{ex}. Initially, $\Gamma_{ex}^{(1)}$ was set at zero and was gradually released to achieve a better fit. The value of Γ_0 was not well determined during the fit, being buried under the exciton line shape. It was constrained to be the same as the linewidth of the fundamental exciton. Other constraints were tried, but led to worse fits. Finally, $\sigma=27\%$ was achieved. (See Table II for the final values.) This is a significant improvement from $\sigma=55\%$, obtained from the fit without the effect of excitons.

Although the spectral data were taken in steps of 5 meV and the excitonic effect is buried under other band-to-band transitions, Eq. (8) enables us to determine the value for E_{ex} at room temperature. Venghaus reported 17.4 meV for E_{ex}, which was obtained by the magnetoreflectance measurement at liquid He temperature.[35] The accurate determination was made possible, since the spectral peaks from the first and second excited state of the excitons were clearly distinguished at low temperature. From the same paper, the average value of 19 meV could be deduced for the excitonic binding energy at low temperature. Our result 13 meV is lower than 19 meV and can be understood in light of the temperature effect. Excitons are thermally unstable at 300 K in emission, and severely broadened in absorption by LO phonons. We are not aware of any literature value for E_{ex} at room temperature. We, however, can roughly estimate the temperature effect. The change in the excitonic binding energy is given by the temperature dependence of the effective mass and the dielectric constant.[36] The former is mainly due to the change in the band gap from 2.82 to 2.67 eV, implying about a 5% reduction in the effective mass. The dielectric constant changes from about 8.8 to 9.25. These values imply a binding energy of about 14.9 meV at 300 K, if 17.4 meV is valid at 0 K. Our result 13 meV appears to confirm such a trend. A lower value than 14.9 meV may imply a further reduction of the effective mass from about 5% to about 15% at room temperature. The accuracy of our value, however, is not expected to be as good as that of those determined at low temperature, since the spectral data are obtained in steps of 5 meV and are broad at room temperature. We expect an uncertainty of 1 – 2 meV in our value.

Figure 3 shows the resultant fit to $L_2(\omega_j)$. The solid lines and circles in Fig. 3 show this fit and the spectral data, respectively. The large nonzero values below the band gap are due to the usual, but incorrect, assumption of Lorentzian broadening, as discussed previously.[13] The effect of Gaussian broadening is considered in subsection B below. The better fit to the derivative spectra by Eq. (7) than that of Eq. (6) proves that the excitonic effect in the spectral data is properly taken into account by Eq. (7). The dotted lines in the figure show the contribution from $\epsilon_{ex}(\omega)$ and $H_0(\omega)$ separately. A similar result is found in fitting the spectral data and its derivatives near $E_0+\Delta_0$. So, in preparing the model for $L(w_j)$ in the whole range, $\epsilon_{ex}(\omega)$ of Eq. (7) is introduced at the critical points E_0 and $E_0+\Delta_0$.

B. Modeling

Let us construct the final model for ZnSe, taking excitonic effects into account. We first construct $W_{cv}(E)$. Because $P_{cv}(E)$ is a slowly varying function of E with no singularities, only the analytic structure of $J_{cv}(E)$ is considered. A band structure for ZnSe was calculated by Chelikowski and Cohen.[37] Although $J_{cv}(E)$ can be calculated from the band structure, a rigorous calculation is not necessary for our purpose. In order to obtain the analytic structure of $J_{cv}(E)$, a schematic representation of $J_{cv}(E)$ with a correct description of the analytical properties for each critical point suffices for determining the analytic structure of $W_{cv}(E)$. The four lowest-energy CP's - E_0, $E_0+\Delta_0$, E_1, and $E_1+\Delta_1$ are apparent in the derivative spectra. Table III summarizes the CP's in order of increasing energy and the associated transi-

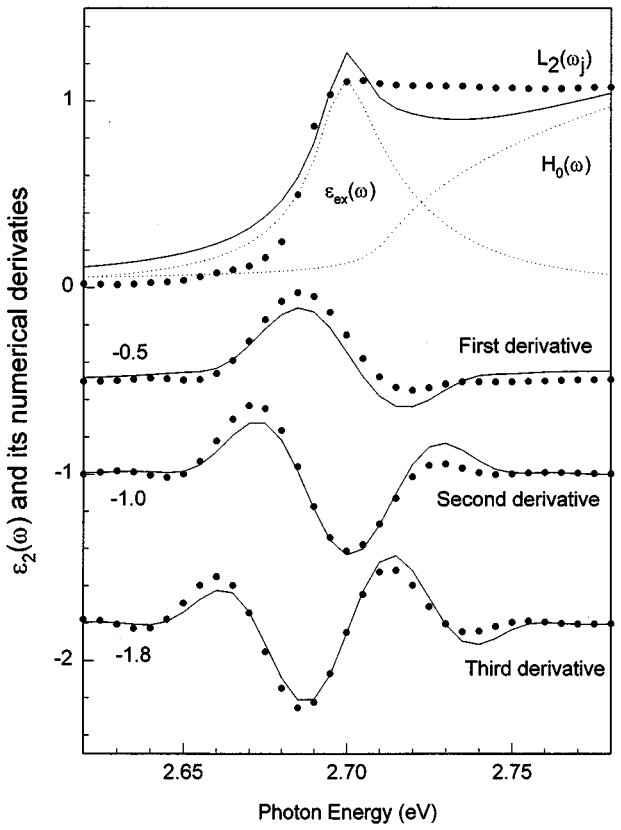

FIG. 3. Fit to $L_2(\omega_j)$ and its derivatives by the use of Eq. (8). The solid lines are the fits. The closed circles (●) are $L_2(\omega_j)$ and its numerical derivatives. The dotted lines show the contributions from ϵ_{ex} and $H_0(\omega)$. The first three derivatives shown are normalized and shifted for comparison. σ is 27%.

tions as calculated by Chelikowski and Cohen.[37] According to this table and from the band structure calculation, a schematic diagram of $J_{cv}(E)$ for each pair of bands can be drawn, which leads to the total $J(E)\equiv\Sigma_{cv}J_{cv}(E)$. Since the details have been shown previously,[13–15] the diagrams are not shown in this paper.

Combining $J(E)$ with $P(E)^2$ leads to $W(E)$. The structure of $W_{cv}(E)$ between E_0 and E_1 is determined by the 3D M_0 type CP's at E_0 and at $E_0+\Delta_0$, and the 3D M_1 type at E_1. Thus, in the first segment $W_{cv}(E)$ has the form

$$W_I(E)=p_I(E)\sqrt{E-E_0}+q_I(E)\sqrt{E-E_0}\sqrt{E_1-E}+r_I(E)\sqrt{E-(E_0+\Delta_0)}, \tag{9}$$

TABLE III. Critical-point (CP) types and their energy values based on the band structure calculation by Chelikowski and Cohen (Ref. 37). CP's are selected in order of increasing energy.

Energy gap (eV)	Transition	CP	3D type
2.76 eV	$\Gamma_8^v\rightarrow\Gamma_6^c$	E_0	M_0
3.21 eV	$\Gamma_7^v\rightarrow\Gamma_6^c$	$E_0+\Delta_0$	M_0
4.72 eV	$L_{4,5}^v\rightarrow L_6^c$	E_1	M_1
5.00 eV	$L_6^v\rightarrow L_6^c$	$E_1+\Delta_1$	M_1
6.50 eV	$X_7^v\rightarrow X_6^c$	E_2	M_1

where $p_I(E)=\Sigma_n p_{I,n}E^n$, $q_I(E)=\Sigma_n q_{I,n}E^n$, and $r_I(E)=\Sigma_n r_{I,n}E^n$. The structure of $W_{cv}(E)$ between E_1 and $E_1+\Delta_1$ is determined by the 2D M_0 type CP at E_1 and the 3D M_1 type at $E_1+\Delta_1$. In this region, Adachi and Taguchi[8] ascribed the entire optical response to excitons, ignoring the contribution from band-to-band transitions, and thus greatly overestimated the contribution from excitons. In our model for this high-energy region, the excitonic effect is not explicitly taken into account, since its effect, if present at all, is considered to be much smaller than that of the lower band transitions. Also, the 2D M_0 nature of the CP at E_1, which leads to a discontinuity, effectively masks any exciton effect. Thus, in the second segment, $W_{cv}(E)$ is taken to have the form

$$W_{II}(E)=p_{II}(E)+q_{II}(E)\sqrt{E_1+\Delta_1-E}. \tag{10}$$

The structure of $W_{cv}(E)$ between $E_1+\Delta_1$ and E_2 is determined by the 2D M_0 type CP at $E_1+\Delta_1$ and the 3D M_1 type at E_2. Again, neglecting exciton effects in the same way as, in this segment, $W_{cv}(E)$ has the form

$$W_{III}(E)=p_{III}(E)+q_{III}(E)\sqrt{E_2-E}. \tag{11}$$

Here, $W(E)=\Sigma_{\nu=I}^{\nu=III}W_\nu(E)$ is terminated at E_2 although it is, in principle, not limited. This cutoff required the introduction of polynomial terms in $\epsilon_1(\omega)$ in our first applications.[13,14] Obviously, the polynomial terms were added to compensate for the contribution to $\epsilon_1(\omega)$, from $W(E)$ above the upper limit of the spectral data. As discussed previously,[15] it is plausible to mimic $\epsilon_2(\omega)$ above the given spectral range by setting a two-dimensional discontinuity at 10 eV. Then, the 2D M_0 type CP at E_2 leads to the form

$$W_{IV}(E)=p_{IV}(E), \tag{12}$$

for $W_{cv}(E)$ in the fourth segment.

We now consider the integration over energy in Eqs. (1) and (2). For the case of Lorentzian line broadening, the substitution of $W(E)=\Sigma_{\nu=I}^{\nu=IV}W_\nu(E)$ into Eq. (1) leads to the equation

$$\epsilon_W(\omega)=1-\frac{8\pi\hbar^2e^2}{m^2}\sum_n\left[(p_nH_n+q_nF_n+r_nH_n)_I+(p_nG_n+q_nK_n)_{II}+(p_nG_n+q_nK_n)_{III}+(p_nG_n)_{IV}\right]. \tag{13}$$

where H_n, F_n, G_n, and K_n are functions of ω, as defined in the previous paper.[13] Now we add the excitonic line shape at E_0 and $E_0+\Delta_0$. This leads to the final model,

$$\epsilon(\omega)=\epsilon_W(\omega)+\epsilon_{ex}(\omega)[E_0]+\epsilon_{ex}(\omega)[E_0+\Delta_0]. \tag{14}$$

The case of Gaussian line broadening is not as simple, since the integral in Eq. (2) cannot be performed analytically. However, the substitution of the quantity[13]

$$D_i=\Gamma_i\exp\left[-\alpha_i\left(\frac{\hbar\omega-E_i}{\Gamma_i}\right)^2\right] \tag{15}$$

for Γ_i in H_n, F_n, G_n, K_n, and ϵ_{ex} leads to analytic functions, which closely mimic the numerical results for the Gaussian case, for appropriate values of α_i. The value of α_i, which most closely mimics the exact results of Gaussian

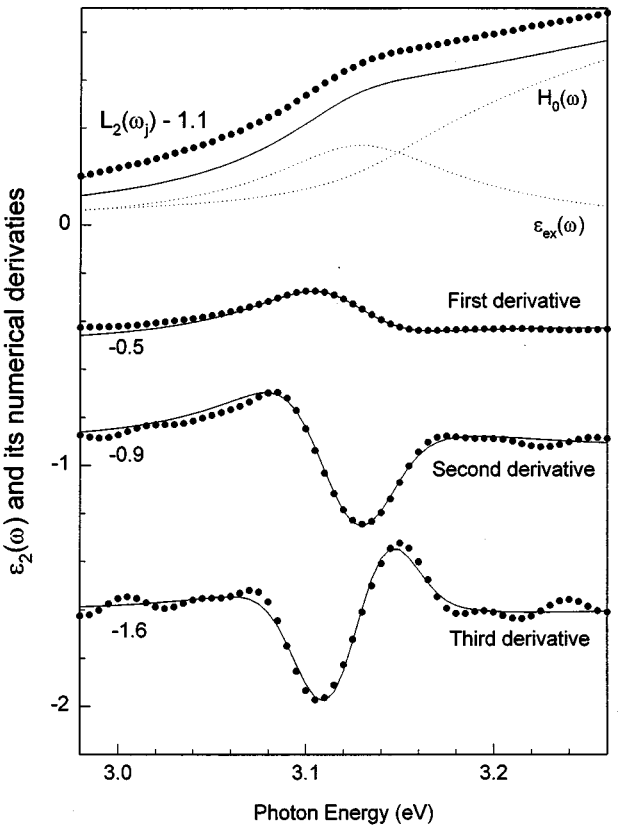

FIG. 4. Fit to the first three derivatives of $L_2(\omega_j)$ by the use of Eq. (8) near $E_0+\Delta_0$. The solid lines are the fits. The closed circles (●) are $L_2(\omega_j)$ and its numerical derivatives. The dotted lines show the contributions from ϵ_{ex} and $H_0(\omega)$. The first three derivatives shown are normalized and shifted for comparison. $(\sigma_1+\sigma_2+\sigma_3)/3$ is 19%.

broadening, is not exactly the same for the four functions H_n, F_n, G_n, and K_n and depends slightly on the value of n, but is approximately 0.2 in all cases.

IV. FITTING OF $L(\omega)$ AND EXTRAPOLATION OF $\epsilon(\omega)$ TO HIGHER AND LOWER ENERGIES

Three steps are taken to fit $L(\omega)$. The first step is to determine the critical-point and excitonic parameters at E_0 and $E_0+\Delta_0$. Those values at E_0 are determined through fitting $L_2(\omega_j)$ and its derivatives over the photon energy range near the band gap, as described previously. For the determination of critical-point parameters, either the second derivative or the third derivative of the spectral data is sufficient. The main reason for introducing the spectral data and its first derivative in the fitting is to determine accurately the strength C_{ex} in the first step. The critical points and excitonic parameters at $E_0+\Delta_0$ are determined through fitting the first three derivatives of $L_2(\omega_j)$ over the photon energy range near $E_0+\Delta_0$. $L_2(\omega_j)$ itself is not used in this fitting, since it contains a large background from other band-to-band transitions. E_{ex} at $E_0+\Delta_0$ is slightly larger for the best fit than its value at E_0, but is fixed at the same value as E_{ex} at E_0, since it is expected to be either lower than or equal to that value for E_{ex} at E_0. Figure 4 shows the resultant fit to the first

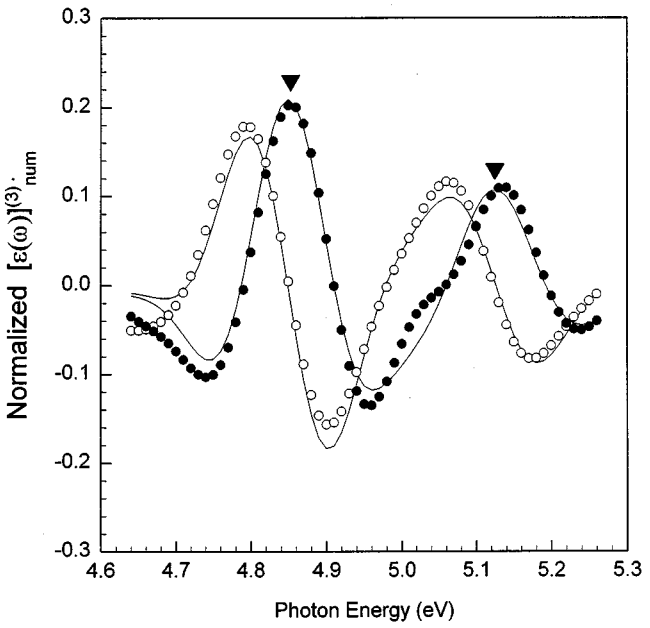

FIG. 5. Fit to $[L(\omega_j)]^{(3)}_{num}$ in the E_1 region. The open (○) and closed (●) circles show $[L_1(\omega_j)]^{(3)}_{num}$ and $[L_2(\omega_j)]^{(2)}_{num}$, respectively. The solid lines show the best fits. The inverted triangles show the positions of critical points.

three derivatives of $L_2(\omega_j)$. The solid lines and circles are the fits and the data, respectively. $(\sigma_1+\sigma_2+\sigma_3)/3$ is 19%. The contributions from $\epsilon_{ex}(\omega)$ and $H_0(\omega)$ are shown separately by the dotted lines. Their summation shown by the solid line is not the result of the direct fit to $L_2(\omega_j)$, but resembles closely the spectral data after removing a constant background. Table II summarizes values for the critical point and excitonic parameters at E_0 and $E_0+\Delta_0$.

The second step is to determine the critical-point parameters at E_1, and $E_1+\Delta_1$. In this step, the number of coefficients $p_{\nu,n}$, $q_{\nu,n}$ and $r_{\nu,n}$ is reduced to a minimum, since the major interest is in the determination of the critical-point parameters. In order to achieve faster convergence, $[L(\omega_j)]^{(3)}_{num}$ is chosen for the fit. If necessary, the photon energy range is also reduced just to include the critical-point structures of interest. Figure 5 shows the resultant fit. σ_3 is 19%. The fit is obtained by using three parameters for each CP – C_i, E_i, and Γ_i. The total number of parameters is 6, which is even less than those used in the critical-point model, which requires a total of eight parameters[9] for two CP's. The values for E_2 and Γ_{E_2} are not determined by the fit, since E_2 is located above the spectral data. E_2 is calculated to be 6.5 eV by Chelikowski and Cohen.[37] The CP energies up to $E_1+\Delta_1$ reported by them are consistently lower by about 100 meV than are our values. So, E_2 is fixed at 6.6 eV. Γ_{E_2} is fixed at 156 meV, following approximately the order of increase among the linewidths as a function of photon energy.

Table IV shows the values of E_i and Γ_i obtained in the first two steps and compares them with the values reported by others. Kim *et al.*[9] reported values for all of the E_i and Γ_i from the analysis of their spectral data. They fitted the second derivative of their data with the appropriate theoreti-

TABLE IV. Comparison of literature values of E_i and Γ_i with ours. The values of E_i and Γ_i are given in units of eV and meV, respectively. The first two columns of values were found from Adachi and Taguchi (Ref. 8) and Kim *et al.* (Ref. 9).

CP	Ref. 8	Ref. 9	This work
E_0	2.69 eV	2.69 eV	2.711 eV
$E_0+\Delta_0$	3.10	3.11	3.139
E_1	4.92	4.83	4.853
$E_1+\Delta_1$	5.22	5.10	5.125
$E_1+\Delta_1$	5.22	5.10	5.125
E_2			6.6
Γ_{E_0}	30 meV	69 meV	5 meV
$\Gamma_{E_0+\Delta_0}$	30	80	37
Γ_{E_1}	370	140	74
$\Gamma_{E_1+\Delta_1}$	370	170	98
Γ_{E_2}			156

cal line shape.[38,39] Notice the large discrepancy in the values of E_0 and $E_0+\Delta_0$ between theirs and ours. Their theoretical line shape did not explicitly include the effect of excitons. Their critical-point energies at E_0 and $E_0+\Delta_0$ are generally lower than ours and become close to our values after subtracting $E_{\rm ex}$ from ours. Besides, their method does not take account of the errors, due to the distortion by numerical differentiation.[32] The large discrepancy between their values for linewidths and ours, especially at the band gap, where the linewidth is very small, arises from those errors. The values reported by Adachi and Taguchi[8] are obtained from fitting their undifferentiated spectral data. So, their critical point parameters are not expected to be accurately determined unless they are fixed to the known values. The values for Γ_{E_1} and $\Gamma_{E_1+\Delta_1}$ found by Adachi and Taguchi[8] are extraordinary high. The differences between our values and theirs are due to the different approaches used in determining the CP parameters.

Having found the values for the E_i, Γ_i, $C_{\rm ex}$, $E_{\rm ex}$, and $\Gamma_{\rm ex}$, we proceed to the final step. In this step, the $p_{n,\nu}$, $q_{n,\nu}$, and $r_{\nu,n}$ are redetermined by minimizing σ_0^2, using Eq. (13) and the values for E_i, Γ_i, $C_{\rm ex}$, $E_{\rm ex}$, and $\Gamma_{\rm ex}$ determined in the first and second steps. This is done in order to obtain a best fit to $L(\omega_j)$ with the critical point and excitonic parameters fixed at their correct values. The final step is very quick because $\epsilon(\omega)$, as in Eq. (13), is a linear function of the $p_{\nu,n}$, $q_{\nu,n}$, and $r_{\nu,n}$, so that they are determined exactly in only one iteration. The value for $r_{\rm I,0}$ is fixed at the value determined in the first step, since its contribution is small. 13 free parameters among the $p_{\nu,n}$, $q_{\nu,n}$, and $r_{\nu,n}$ are chosen. A further increase in the number of free parameters results in only a small decrease in σ_0. Upon keeping Lorentzian broadening, we find the fit to $L(\omega_j)$ shown as the solid lines in Fig. 6 between 1.5 eV and 6.0 eV. σ_0 is 1.8%. The corresponding best-fit values of the $p_{n,\nu}$, $q_{n,\nu}$, and $r_{\nu,n}$ are given in Table V.

Discrepancies are notable between $L_1(\omega_j)$ and the fit below the band gap. $\epsilon_1(\omega)$ shows a strong cusp around E_0 as in $L_1(\omega_j)$, but is consistently lower than $L_1(\omega_j)$ below E_0. The result is considered to be only a poor fit, but the fit is close to the data of Marple[16] in that region. Table I lists the results at 1.5 eV, 2.5 eV, and 2.6 eV for numerical comparison. The better agreement between the fit and the data of Marple suggests that the calculated $\epsilon_1(\omega)$ constrained to satisfy the Kramers-Kronig relationship may be better than the

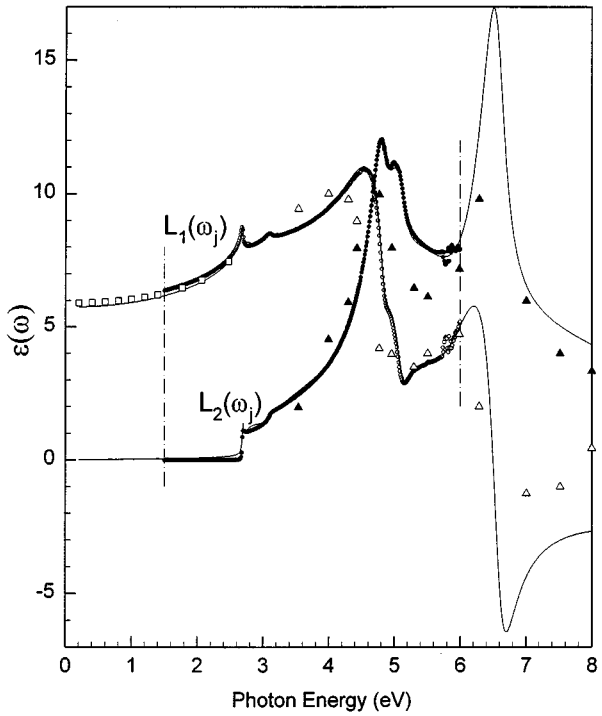

FIG. 6. Comparison of $L(\omega_j)$ and other data with $\epsilon(\omega)$ extended beyond the spectral limit. The open (○) and closed (●) circles show $L_1(\omega_j)$ and $L_2(\omega_j)$, respectively. The boundaries at 1.5 eV and 6.0 eV indicate the photon energy limit of $L(\omega_j)$ used for the fit. The solid lines show the calculation of $\epsilon(\omega)$ extended beyond the spectral data limit. The open and closed triangles show the real and imaginary parts of the dielectric function for bulk ZnSe obtained by Cardona (Ref. 26). The open squares show the real part of the dielectric function for bulk ZnSe obtained by Marple (Ref. 16).

TABLE V. Values of the coefficients $p_{\nu,n}$, $q_{\nu,n}$, and $r_{\nu,n}$, determined in each region through fitting $L(\omega_j)$, which are multiplied by $8\pi\hbar^2e^2/m^2$. The zero values were fixed to reduce the number of free parameters.

Polynomial function	Order 0	Order 1	Order 2
$p_{{\rm I},n}$	-0.19596×10^5	0.74707×10^4	-0.70365×10^3
$q_{{\rm I},n}$	0.9185×10^4	-0.27039×10^4	0.16824×10^3
$r_{{\rm I},n}$	0.71056×10^1	0	0
$p_{{\rm II},n}$	0.16274×10^3	0	0
$q_{{\rm II},n}$	-0.18906×10^3	0	0
$p_{{\rm III},n}$	0.23612×10^5	-0.34069×10^4	0
$q_{{\rm III},n}$	-0.11037×10^5	0.11750×10^4	0
$p_{{\rm IV},n}$	0.88943×10^2	0	0

data in this region. Higher values of $\epsilon(\omega)$ than those of $L(\omega_j)$ are observed right above the band gap. This is caused by trying to fit $L_1(\omega_j)$ below E_0, where most of the discrepancies occur. Thus, the fit was further improved when the fitting range was limited to the range above 1.5 eV. For example, σ_0 was 1.6% in the range between 2.5 eV and 6 eV. Clearly, the fit to $L(\omega_j)$ above the band gap was improved. In any case, the deviation is substantially smaller than the rms deviation in the fit made by Adachi and Taguchi.[8] As previously discussed,[13,14] the resulting fit to $L_2(\omega_j)$ with purely Lorentzian broadening did not yield a good fit, especially below E_0. The introduction of Gaussian broadening was necessary to improve the calculation of $\epsilon_2(\omega)$ below E_0. The method and results were discussed in detail previously[13–15] and are not presented in this paper.

Having calculated $\epsilon(\omega)$ in the spectral range, it is easily extrapolated beyond the spectral limit. The solid lines in Fig. 6 show $\epsilon(\omega)$ between 0.2 eV and 8 eV. The boundaries at 1.5 eV and 6.0 eV show the limits of the $L(\omega_j)$ data used for the fit. The open squares in this figure show the results of Marple.[16] $\epsilon_1(\omega)$ below the lower limit down to 0.2 eV is also close to the results of Marple. $\epsilon(\omega)$ above the spectral limit also shows a reasonable optical response around the E_2 region in light of other optical dielectric functions in the E_2 region. The ratio of $\epsilon_2(\omega)$ in the E_1 region to that in the E_2 region is similar to that in the dielectric function of other semiconductor materials. The maximum value of $\epsilon_2(\omega)$ is on the order of 15 in the E_2 region, which is commensurate to the theoretical value of Wang and Klein[17] and a little higher than the experimental value cited in the same paper. The open and closed triangles in this figure show results of Cardona.[26] Having calculated $\epsilon(\omega)$ between 0.2 eV and 8 eV, other optical properties, such as refractive indices and absorption coefficients in those regions, can be easily calculated using standard formulas.

V. CONCLUSIONS

We have obtained the spectral data of thin film ZnSe grown on GaAs (100), using spectroscopic ellipsometry. The spectral data show four distinctive critical-point structures, including the weak structures at $E_0+\Delta_0$ and $E_1+\Delta_1$, indicating that the sample has a high crystalline quality. The optical dielectric function for bulk ZnSe is deduced, using the standard multilayer analysis together with our technique, which will be presented elsewhere. The resultant data are better in several points than those reported by Kim *et al.*[9] The spectral data reveal the evidence of excitonic effects at E_0 and $E_0+\Delta_0$, which cannot be described by the usual 3D M_0 type critical point. We have developed the excitonic line shape and have incorporated it properly in our existing model. This enables us to determine 13 meV for $E_{\rm ex}$ at room temperature. As embodied in our original model, $\epsilon_{\rm ex}(\omega)$ is also capable of describing the spectral data and its derivatives simultaneously. Having incorporated the excitonic effect in the existing model, we have not only determined the room-temperature CP and excitonic parameters accurately, but have also obtained an accurate analytical expression for $\epsilon(\omega)$. The calculation automatically satisfies the Kramers-Kronig relation between the real and imaginary parts of $\epsilon(\omega)$. This expression is accurate from 0.2 eV up to 6 eV, as revealed by comparison with other spectroscopic data, and is approximately valid even above 6.0 eV.

ACKNOWLEDGMENTS

The authors are grateful to L. A. Almeida and J. W. Garland, who read this manuscript and gave their valuable comments. The authors are grateful to B. J. Skromme who gave a comment on the exciton binding energy. The authors are also grateful to the National Science Foundation for its support under Grant No. ECS-9202664 and to the Office of Naval Research under Grant No. N00014-95-1-0349.

[1] H. Morkoç, S. Strite, G. B. Gao, M. E. Lin, B. Sverdlov, and M. Burns, J. Appl. Phys. **76**, 1363 (1994).
[2] G. F. Neumark, R. M. Park, and J. M. Depuydt, Phys. Today **47** (6), 26 (1994).
[3] R. L. Gunshor and A. V. Nurmikko, MRS Bull. **20** (7), 15 (1995).
[4] S. Itoh and A. Ishibashi (unpublished).
[5] J. I. Pankove, *Optical Processes in Semiconductors* (Dover, New York, 1975).
[6] D. E. Aspnes, W. E. Quinn, and S. Gregory, Appl. Phys. Lett. **57**, 2707 (1990).
[7] L. Ward, in *Handbook of Optical Constants of Solids II*, edited by E. D. Palik (Academic, New York, 1991), p. 737, and references therein.
[8] S. Adachi and T. Taguchi, Phys. Rev. B **43**, 9569 (1991).
[9] Y. D. Kim, S. L. Cooper, and M. L. Klein, Appl. Phys. Lett. **62**, 2387 (1993).
[10] C. C. Kim, P. M. Raccah, and J. W. Garland, Rev. Sci. Instrum. **63**, 2958 (1992).
[11] D. E. Aspnes, in *Optical Properties of Solids*, edited by B. O. Seraphin (North-Holland, Amsterdam, 1976), p. 800.
[12] R. M. A. Azzam and N. M. Bashara, *Ellipsometry and Polarization Light* (North-Holland, New York, 1977).
[13] C. C. Kim, J. W. Garland, and P. M. Raccah, Phys. Rev. B **45**, 11 749 (1992).
[14] C. C. Kim, J. W. Garland, and P. M. Raccah, Phys. Rev. B **47**, 1876 (1993).
[15] C. C. Kim and S. Sivananthan, J. Appl. Phys. **78**, 4003 (1995).
[16] D. T. F. Marple, J. Appl. Phys. **35**, 1241 (1964).
[17] C. S. Wang and B. M. Klein, Phys. Rev. B **24**, 3417 (1981).
[18] B. J. Skromme, Y. Zhang, W. Liu, B. Parameshwaran, D. J. Smith, and S. Sivananthan, in *Better Ceramics Through Chemistry VI*, edited by A. K. Cheetham, C. J. Brinker, M. L. Mecartney, and C. Sanchez, MRS Symposia Proceedings No. 326 (Materials Research Society, Pittsburgh, 1994), p. 15.
[19] V. M. Bermudez and V. H. Ritz, Appl. Opt. **17**, 15 (1978).
[20] T. Taguchi, I. Kodguchi, and H. Nanba, U.S. Patent No. 4,866,007 (September 1989).

[21] D. E. Aspnes, in *The Accurate Determination of Optical Properties by Ellipsometry*, edited by E. D. Palik (Academic, New York, 1985), Chap. 5, p. 89.
[22] I. H. Malitson, J. Opt. Soc. Am. **55**, 1205 (1965).
[23] D. E. Aspnes, G. P. Schwartz, G. J. Gualtieri, A. A. Studna, and B. Schwartz, J. Electrochem. Soc. **128**, 590 (1981).
[24] H. Arwin and D. E. Aspnes, J. Vac. Sci. Technol. A **2**, 1316 (1984).
[25] H. Yao and P. G. Snyder, Thin Solid Films **206**, 283 (1991).
[26] M. Cardona, in *Proceedings of the International Conference on Physics of Semiconductors*, edited by M. Hulin (Academic Press, New York, 1964), p. 181.
[27] R. Del Sole and D. E. Aspnes, Phys. Rev. B **17**, 3310 (1977).
[28] D. E. Aspnes and A. A. Studna, Appl. Phys. Lett. **39**, 316 (1981).
[29] M. D. Struge, Phys. Rev. **127**, 768 (1962).
[30] J. E. Potts, H. Cheng, S. H. Park, B. Fluegel, M. Joffre, S. W. Koch, and N. Peyhgambarian, Proc. SPIE **881**, 107 (1988).
[31] A. Savitsky and M. J. E. Golay, Anal. Chem. **36**, 1627 (1964).
[32] J. W. Garland, C. C. Kim, H. Abad, and P. M. Raccah, Phys. Rev. B **41**, 7602 (1990).
[33] J. W. Garland, C. C. Kim, H. Abad, and P. M. Raccah, Thin Solid Films **233**, 148 (1993).
[34] R. J. Elliott, Phys. Rev. **108**, 1384 (1957).
[35] H. Venghaus, Phys. Rev. B **19**, 3071 (1979).
[36] C. Kittel, *Introduction to Solid State Physics* (Wiley, New York, 1976).
[37] J. R. Chelikowski and M. L. Cohen, Phys. Rev. B **14**, 556 (1976).
[38] M. Cardona, in *Solid State Physics: Advances in Research and Applications*, edited by F. Seitz, D. Turnbull, and H. Ehrenreich (Academic, New York, 1969), Vol. 11.
[39] D. E. Aspnes, in *Handbook on Semiconductors*, edited by M. Balkanski (North-Holland, Amsterdam, 1980), Vol. 2, p. 109.